## COMMUNICATION

Check for updates

# Slow magnetic relaxation influenced by change of symmetry from ideal $C_i$ to $D_{3d}$ in cobalt(II)-based single-ion magnets†

Lei Chen,[a] Jianjun Zhou,[a] Hui-Hui Cui,[b] Ai-Hua Yuan, [iD] *[a] Zhenxing Wang, [iD] *[c] Yi-Quan Zhang,*[d] Zhong-Wen Ouyang[c] and You Song [iD] *[b]

The coordination geometries of the Co(II) site in the two complexes [Co(imidazole)$_6$][BPh$_4$]$_2$·0.3CH$_3$CN (1) and [Co(imidazole)$_6$][NO$_3$]$_2$ (2) were observed to display the ideal symmetries $C_i$ and $D_{3d}$, respectively. Both complexes were shown to be field-induced single-ion magnets. The effective energy barrier was found to decrease as the local symmetry changed from low-symmetry $C_i$ to high-symmetry $D_{3d}$.

The study of single-ion magnets (SIMs) has been a burgeoning and hot topic in molecular magnetism since the first discovery of slow magnetic relaxation in a mononuclear lanthanide complex.[1] In this regard, several breakthroughs based on lanthanide SIMs have recently been reported, with these breakthroughs possible due to their large unquenched orbital angular momentum and strong spin–orbit coupling.[2] An amazing advance has been made here: an energy barrier of 1837 K and a magnetic blocking temperature of 60 K have been achieved for a dysprosium metallocene complex [(Cp$^{ttt}$)$_2$Dy] [B(C$_6$F$_5$)$_4$], the largest values yet discovered for SIMs.[2e,f] Although the prolific lanthanide-based SIMs show high performance,[2] research about SIMs with a d metal center (d-SIMs) has also attracted considerable attention. Most of the reported d-SIMs based on iron(I,II,III), cobalt(II), manganese(III), nickel(I,II), rhenium(IV), chromium(II), and iridium(IV) ions have coordination numbers ranging from 2 to 6.[3–13] In these cases, the low coordination environment is believed to produce a weak ligand field, thus enhancing the magnetic anisotropy. However, several examples of seven- and eight-coordinate geometries showing slow magnetic relaxation behavior have been found. We previously discovered the first eight-coordinate SIM and a series of seven-coordination Co(II)-based SIMs.[14] Gao *et al.* reported an eight-coordinate Fe(II)-based SIM having a highly distorted dodecahedron geometry.[15] Meanwhile, a few mononuclear seven-coordination Co(II) and Fe(II) complexes have also been reported to display slow magnetic relaxation.[16]

Besides the excellent performance (high energy barrier and blocking temperature) of SIMs compared to the polynuclear systems, the SIMs are conductive to investigate their magneto-structural relationship. As a representative example, Long *et al.* have studied the effect of different coordinating atoms on magnetic properties of the tetrahedral cobalt complexes [Co(EPh)$_4$]$^{2-}$ (E = O, S, and Se), and revealed the softer donor atoms S and Se to facilitate a greater magnetic anisotropy.[7b] A similar trend was also reported by the Dunbar[7c] and Wang groups.[16a] Moreover, Vaidya *et al.* found that the zero-field splitting parameter ($D$) was switched from positive to negative, with the substitution of the donor O atom by the S atom.[7d] These studies demonstrated the ability to tune the magnetic anisotropy by using ligands with the different donor atoms. It is well known that the coordination environment factors that influence the magnetic properties not only include the identity of the donor atom but also the local symmetry around the metal centers. However, it is difficult to investigate the relationship between symmetry of a ligand field and the magnetic properties in the same coordination geometry, because the degree of geometry distortion cannot be easily controlled, and small changes in the local structure may lead to considerable changes in the magnetic properties. Therefore, designing a tiny change of the ligand field is desired, and may deepen our understanding of the magneto-structural relationship of SIMs. With this in mind, we used the imidazole molecule as the sole ligand together with different counter anions to construct two simple mononuclear cobalt complexes: [Co(imidazole)$_6$][BPh$_4$]$_2$·

*[a]School of Environmental and Chemical Engineering, Jiangsu University of Science and Technology, Zhenjiang 212003, P. R. China. E-mail: aihua.yuan@just.edu.cn*
*[b]State Key Laboratory of Coordination Chemistry, Nanjing National Laboratory of Microstructures, School of Chemistry and Chemical Engineering, Nanjing University, Nanjing 210093, P. R. China. E-mail: yousong@nju.edu.cn*
*[c]Wuhan National High Magnetic Field Center & School of Physics, Huazhong University of Science and Technology, Wuhan 430074, P. R. China.*
*E-mail: zxwang@hust.edu.cn*
*[d]Jiangsu Key Laboratory for NSLSCS, School of Physical Science and Technology, Nanjing Normal University, Nanjing 210023, P. R. China.*
*E-mail: zhangyiquan@njnu.edu.cn*
†Electronic supplementary information (ESI) available: Detailed crystallographic data, XRD patterns, and magnetic data. CCDC 1583132–1583133. For ESI and crystallographic data in CIF or other electronic format see DOI: 10.1039/c7dt04651k

0.3CH$_3$CN (**1**) and [Co(imidazole)$_6$] [NO$_3$]$_2$ (**2**). The [Co(imidazole)$_6$]$^{2+}$ cations in **1** and **2** were each determined to display a quasi-octahedral geometry, with the ideal symmetries $C_i$ and $D_{3d}$, respectively. Both complexes showed typical SIM behavior. Impressively, the effective energy barriers improved with the reduction of the ligand field symmetry from $D_{3d}$ to $C_i$. Interestingly, the high and ideal $D_{3d}$ symmetric coordination environment with six identical Co–N lengths in **2** resulted in uniaxial anisotropy and thus slow magnetic relaxation behavior. In this work, while the changes upon ligand substitution were curbed in both complexes, the different local symmetries of the Co(II) ion originating from the subtle change of bond lengths and angles were employed to analyze the magneto-structural relationship. To the best of our knowledge, this work represents the first observation of the influence of ideal symmetry on magnetic properties in the area of d-SIMs.

The molecular structures of **1** and **2** were determined by taking single-crystal X-ray diffraction measurements. The parameters of the single-crystal structural analyses and the selected bond lengths and bond angles in the CoN$_6$ coordination polyhedrons for both complexes are shown in Tables S1 and S2.† Complexes **1** and **2** crystallized in the monoclinic space group $C2/c$ and rhombohedral space group $R\bar{3}$, respectively. The structures of their cations were found to be very similar (as shown in Fig. 1), with the central Co(II) ion in both cases coordinated with six imidazole nitrogen atoms to form an octahedral configuration. For **1**, the bond lengths of Co–N1, Co–N3, and Co–N5 were measured to be 2.1496(13), 2.1834(13), and 2.1772(13) Å, respectively, which suggested a distorted octahedron with pronounced compression along the N1–Co1–N1a bond due to the Jahn–Teller effect. However, in **2**, we found the six imidazole ligands to be crystallographically equivalent, with the Co–N bond lengths all 2.1618(10) Å. We measured the ranges of the angles between two adjacent Co–N bonds in **1** and **2** to be 87.79(5)–92.21(5)° and 88.23(4)–91.77(4)°, respectively, and all of the angles formed by two diagonal N atoms and the central Co ions to be equal to the ideal value 180° in both complexes. The continuous-shape-measurement (CSM) analyses using SHAPE 2.0 software showed small values (0.039 for **1** and 0.048 for **2**) relative to the octahedron,[17] suggesting their CoN$_6$ coordination geometries to be very close

to $O_h$ symmetry. Interestingly, the CoN$_6$ polyhedrons for **1** and **2** were found to belong to the ideal $C_i$ and $D_{3d}$ point groups, respectively, with the coordination environment around the Co ion in **2** being much more symmetric than in **1**. In addition, the distances between the nearest-neighbor Co(II) ions were measured to be 11.5043(13) Å for **1** and 8.6756(18) Å for **2**, demonstrating no close intermolecular exchange pathways.

The PXRD patterns confirmed a correspondence between all samples used for the magnetic measurements and those simulated from single-crystal X-ray diffraction data (Fig. S1 and S2†). Dc magnetic susceptibility data of crystalline powder samples of **1** and **2** were collected between 2 and 300 K (Fig. 2). The experimentally determined $\chi_M T$ values of 3.05 cm$^3$ K mol$^{-1}$ for **1** and 3.25 cm$^3$ K mol$^{-1}$ for **2** at 300 K were consistent with an $S = 3/2$ spin center with $g = 2.55$ and 2.63, respectively, and significantly exceeded the spin-only value (1.875 cm$^3$ K mol$^{-1}$), thus revealing the strong orbital contribution. Upon cooling, $\chi_M T$ remained nearly constant with only a little decrease as the temperature was cooled from 300 to 150 K, but with a sharp decrease below 150 K to the minimum values of 1.67 cm$^3$ K mol$^{-1}$ for **1** and 1.89 cm$^3$ K mol$^{-1}$ for **2** at 2 K. Magnetization *versus* field curves were determined for the temperature range 1.8 to 5 K under applied magnetic fields of 0–7 T. At 2 K, the magnetizations were nearly saturated at 70 kOe, reaching values of 2.33$N\mu_B$ for **1** and 2.40$N\mu_B$ for **2**, considerably less than the calculated value of 3$N\mu_B$ for the spin $S = 3/2$ ground state with $g = 2$ (Fig. S3 and S4†). Their $M$ vs. $H/T$ plots showed only small separations, indicative of an isolated ground state (Fig. 2 inset).

The sign of the magnetic anisotropy is well known to play a crucial role in the magnetic behavior of high-spin Co(II) complexes. The reported hexacoordinated high-spin Co(II) SIMs with quasi-octahedral geometry were observed to display both positive and negative axial anisotropies.[8] Attempts at simultaneously fitting $\chi_M T$ vs. $T$ and $M$ vs. $H/T$ have been unreliable at determining the sign of the magnetic anisotropy. As shown in Fig. 3, the high-frequency electron paramagnetic resonance (HF-EPR) spectra for **1** and **2** recorded at 2 K presented three signals, typical for a spin 3/2 system with the magnitudes of magnetic anisotropy exceeding the frequency
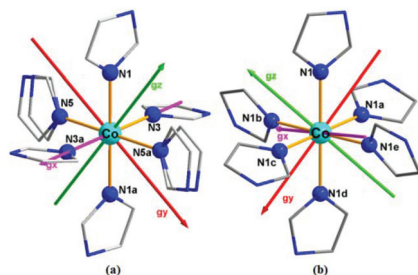


**Fig. 1** Structures of the [Co(imidazole)$_6$]$^{2+}$ cations in **1** (a) and **2** (b). Cyan and blue spheres represent Co and N atoms, respectively. H atoms were omitted for clarity. The arrowed lines represent calculated orientations of the local magnetic axes of the ground-state doublet of Co(II) ion.
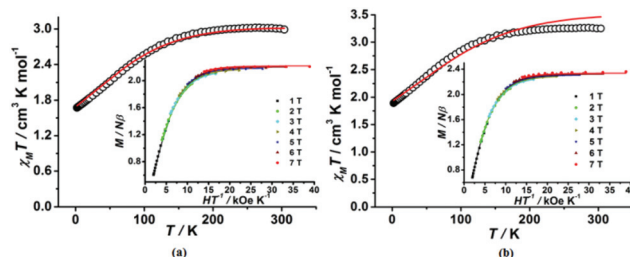


**Fig. 2** Variable-temperature dc susceptibility under a 1000 Oe dc field for **1** (left) and **2** (right) with the solid red lines for PHI fit (red line). Insets: For each case, the corresponding field dependence of magnetization for the temperature range 1.8–5 K. The solid lines represent the fits from PHI software.
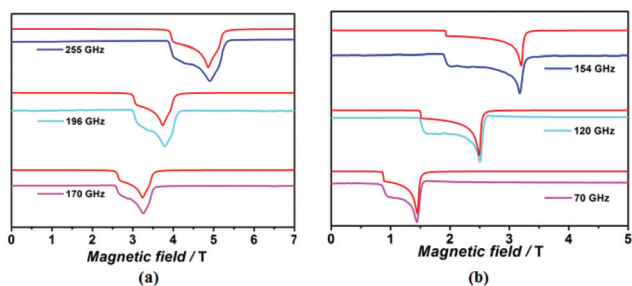
**Fig. 3** HF-EPR spectra of **1** (left) and **2** (right) recorded at 2 K with various microwave frequencies. Each red line represents the best fit obtained by using PHI.[19]

range. The three components were labelled by an effective $S^* = 1/2$, yielding effective $g$ values of $g_{x,\text{eff}} = 3.52$, $g_{y,\text{eff}} = 3.75$, $g_{z,\text{eff}} = 4.61$ for **1** and $g_{x,\text{eff}} = 3.42$, $g_{y,\text{eff}} = 3.43$, $g_{z,\text{eff}} = 5.70$ for **2**. The presence of a lone low-field component ($g_{z,\text{eff}} = 4.61$ for **1** and $g_{z,\text{eff}} = 5.70$ for **2**) well separated from two high-field components ($g_{x,\text{eff}} = 3.52$, $g_{y,\text{eff}} = 3.75$ for **1** and $g_{x,\text{eff}} = 3.42$, $g_{y,\text{eff}} = 3.43$ for **2**) confirmed the easy-axis type magnetic anisotropy in the two complexes. The significant splitting between the two high-field components ($g_{x,\text{eff}}$ and $g_{y,\text{eff}}$) in complex **1** revealed the non-negligible rhombic term. However, the values of $g_{x,\text{eff}}$ and $g_{y,\text{eff}}$ for complex **2** were found to be almost the same, corresponding to the identical Co–N bond lengths.

Considering the strong orbital contribution to the magnetic moment in mononuclear six-coordinated high-spin Co(II) complexes, we employed the Hamiltonian in eqn (1), in order to analyze the DC magnetic properties and EPR data.

$$\hat{H} = \sigma\lambda\hat{L}\cdot\hat{S} + \sigma^2\left(B_2^0(3\hat{L}_z^2 - \hat{L}^2) + \frac{B_2^2}{2}(\hat{L}_+^2 + \hat{L}_-^2)\right) + \mu_B(\sigma\hat{L} + 2\hat{S})\cdot H \tag{1}$$

In eqn (1), $\sigma$ represents a combined orbital reduction parameter and $\sigma = -A\cdot\kappa$, $\lambda$ is the spin–orbit coupling constant, and $B_2^0$ and $B_2^2$ are crystal field parameters (CFPs). Due to the ground-state cubic $^4T_1$ term of the high-spin Co(II) ion ($S = 3/2$), the orbital angular momentum refers to $L = 1$.[18] To avoid over-parameterisation, the spin–orbit coupling constant $\lambda$ value was fixed to $-171.5$ cm$^{-1}$ and the $B_2^0$ parameter must be negative due to the easy-axis anisotropy. The fit to the dc magnetic data resulting from using the PHI program afforded a reasonable set of magnetic parameters, as listed in Table S3.†[19] The fitting curves reproduced the data well, as shown in Fig. 2. The value of the $B_2^2$ parameter for **1** was found to be greater than that for **2**, and this difference corresponded to the difference between the structural rhombic distortions of the two complexes. At the same time, the HFEPR spectra were also well fit based on this model (Table S3† and Fig. 3). As shown in Table S3,† the $B_2^2$ parameters of both complexes obtained from EPR also revealed the changed trend of their structural rhombic distortion. The fitting results from dc magnetic data and EPR for both complexes yielded large negative values of

the axial parameters $B_2^0$, which is characteristic of uniaxial magnetic anisotropy.

To explore the magnetization dynamics and possible presence of a SIM character, ac susceptibility measurements were taken from microcrystalline powders of **1** and **2**. In the absence of a dc field, no out-of-phase ac susceptibility ($\chi''_M$) signals were observed. This result was probably due to quantum tunneling of the magnetization (QTM), as usually observed in d-SIMs. Under applied dc fields, both complexes **1** and **2** showed typical slow magnetic relaxation (Fig. S5 and S6†). The $\chi''_M$ signals intensified and shifted to lower frequencies as the applied dc field was increased up to 1000 Oe, and then weakened at higher fields, with these maxima of the $\chi''_M$ signals for **1** and **2** observed at frequencies of 20.7 and 137.9 Hz, respectively. Our results revealed the magnetic relaxation for **2** to be obviously more rapid than for **1**.

Further ac susceptibility data were collected as a function of both temperature and frequency at 1000 Oe (Fig. 4, and Fig. S7, S8†). Frequency-dependent $\chi''_M$ peaks for **1** were observed between 1–1000 Hz at temperatures from 1.8 to 4.2 K while such peaks were observed only in the low-temperature region (1.8–2.6 K) for **2**. These $\chi''_M$ peak positions were used to extract the relaxation times $\tau$. From an Arrhenius plot of $\ln(\tau)$ vs. $1/T$ (Fig. S9†), we derived the following effective spin-reversal barrier and pre-exponential factors: $U_{\text{eff}} = 21.6$ K, $\tau_0 = 1.5 \times 10^{-6}$ s for **1**, and $U_{\text{eff}} = 6.3$ K, $\tau_0 = 4.5 \times 10^{-5}$ s for **2**. It is notable that a Raman process could make significant contributions in most of the reported Co(II)-based SIMs and a direct one-phonon contribution should not be overlooked at low temperature. The temperature-dependent relaxation times for **1** were calculated from a combination of the Raman and direct relaxation mechanisms according to eqn (2).

$$\tau^{-1} = CT^n + AT \tag{2}$$

As shown in Fig. S10† shows, this mode gave a very good agreement with the experimental data. The best fit yielded $C = 0.56$ S$^{-1}$ K$^{-2}$, $n = 6.1$, and $A = 62.2$ S$^{-1}$ K$^{-1}$. For complex **2**, fewer data points were available for the $\ln(\tau)$ vs. $T^{-1}$ plot, with a more limited temperature range, thus only a Raman process was used to fit the relaxation time, and yielded $C = 115.6$ S$^{-1}$ K$^{-3}$ and $n = 2.9$ (Fig. S11†). The values of $n$ for **1** and **2** were determined to be between 1 and 6, suggesting a considerable contribution of an optical acoustic Raman process in two complexes.
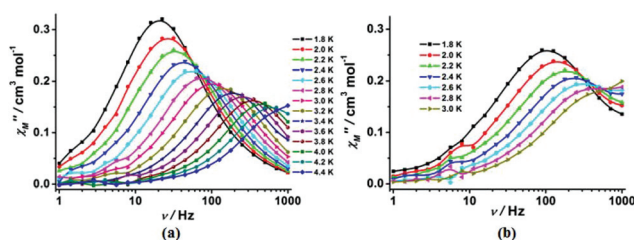


**Fig. 4** Frequency dependence of the ac susceptibility under a dc field of 1000 Oe for **1** (left) and **2** (right). The solid lines are visual guides.

To further evaluate the contrasting magnetic property patterns observed for complexes **1** and **2**, *ab initio* calculations were performed by using the CASSCF/RASSI method (Fig. S12†).[20] The calculated spin-free energies of the lowest ten terms ($S = 3/2$) of the Co(II) ion is shown in Table S4.† The energies of the first excited states (79.5 cm⁻¹ for **1** and 15.0 cm⁻¹ for **2**) and the second excited states (320.7 cm⁻¹ for **1** and 516.8 cm⁻¹ for **2**) were very small, relative to their third excited states of approximately 8000 cm⁻¹. This result indicated the first and second two states to be almost degenerate, in agreement with the small distortion of the structure derived from the Jahn–Teller effect. The five most important spin–orbit-free states mixing with the spin–orbit coupling (SOC) gave rise to the large energy levels of the first excited doublets (273.8 cm⁻¹ for **1** and 241.9 cm⁻¹ for **2**) (Tables S5 and S6†). As mentioned above, these calculated energies of the first excited KD were significantly different from the $U_{eff}$ obtained by the Arrhenius fit. However, it is worth noting that the calculated values were found to be in the same order as the experiment results. Importantly, the energy difference between the lowest two spin-free states (Table S4†) for complexes **1–2** was determined to be much smaller than that between the lowest two spin–orbit states (see Table S6†), and the spin–orbit ground states were all composed of the lowest two spin-free states (see Table S5†). These results indicated the zero-field splitting parameters $D$ and $E$ to be unsuitable for depicting their magnetic anisotropies, in accord with the experimental analyses. The calculated orientations of the $g_x$, $g_y$ and $g_z$ axes on Co$^{II}$ of complexes **1–2** are shown in Fig. 1. The easy axis $g_z$ was determined to be oriented approximately along the $C_2$-axis for **1** and $C_3$-axis for **2**, and perpendicular to the $g_x$ and $g_y$ axes. It is worthwhile noting the sensitivity of the $g_z$ axis orientation to the different coordination environment symmetries.

In conclusion, two mononuclear Co(II) complexes including the same [Co(imidazole)$_6$]$^{2+}$ cation were prepared with a sole ligand (imidazole) and the counter anions BPh$_4$⁻ for **1** and NO$_3$⁻ for **2**. Despite the CoN$_6$ coordination geometries in both complexes having been identified as octahedrons, the local symmetries of the Co(II) centers were manipulated by the counter anion and the guest molecule (CH$_3$CN). The two complexes showed different levels of field-induced slow magnetic relaxation with different effective barrier values (21.6 K for **1** and 6.3 K for **2**), which correspond to the local symmetries from low-symmetry $C_i$ to high-symmetry $D_{3d}$.

## Conflicts of interest

There are no conflicts to declare.

## Acknowledgements

## Notes and references

1 N. Ishikawa, M. Sugita, T. Ishikawa, S.-Y. Koshihara and Y. Kaizu, *J. Am. Chem. Soc.*, 2003, **125**, 8694–8695.

2 (*a*) H. L. C. Feltham and S. Brooker, *Coord. Chem. Rev.*, 2014, **276**, 1–33; (*b*) K. Liu, X. Zhang, X. Meng, W. Shi, P. Cheng and A. K. Powell, *Chem. Soc. Rev.*, 2016, **45**, 2423–2439; (*c*) D. N. Woodruff, R. E. P. Winpenny and R. A. Layfield, *Chem. Rev.*, 2013, **113**, 5110–5148; (*d*) P. Zhang, Y.-N. Guo and J. Tang, *Coord. Chem. Rev.*, 2013, **257**, 1728–1763; (*e*) C. A. P. Goodwin, F. Ortu, D. Reta, N. F. Chilton and D. P. Mills, *Nature*, 2017, **548**, 439–442; (*f*) F.-S. Guo, B. M. Day, Y.-C. Chen, M.-L. Tong, A. Mansikkamäki and R. A. Layfield, *Angew. Chem., Int. Ed.*, 2017, **56**, 11445–11449; (*g*) H. Zhou, Q. Chen, H.-B. Zhou, X.-Z. Yang, Y. Song and A.-H. Yuan, *Cryst. Growth Des.*, 2016, **16**, 1708–1716; (*h*) L. Chen, J. J. Zhou, A.-H. Yuan and Y. Song, *Dalton Trans.*, 2017, **46**, 15812–15818.

3 (*a*) G. A. Craiga and M. Murrie, *Chem. Soc. Rev.*, 2015, **44**, 2135–2147; (*b*) S. Gómez-Coca, D. Aravena, R. Morales and E. Ruiz, *Coord. Chem. Rev.*, 2015, **289–290**, 379–392; (*c*) A. K. Bar, C. Pichon and J.-P. Sutter, *Coord. Chem. Rev.*, 2015, **308**, 346–380; (*d*) J. M. Frost, K. L. M. Harriman and M. Murugesu, *Chem. Sci.*, 2016, **7**, 2470–2491.

4 J. M. Zadrozny, D. J. Xiao, M. Atanasov, G. J. Long, F. Grandjean, F. Neese and J. R. Long, *Nat. Chem.*, 2013, **5**, 577–581.

5 (*a*) C. Mathoniere, H. J. Lin, D. Siretanu, R. Clerac and J. M. Smith, *J. Am. Chem. Soc.*, 2013, **135**, 19083–19086; (*b*) P. H. Lin, N. C. Smythe, S. I. Gorelsky, S. Maguire, N. J. Henson, I. Korobkov, B. L. Scott, J. C. Gordon, R. T. Baker and M. Murugesu, *J. Am. Chem. Soc.*, 2011, **133**, 15806–15809.

6 S. Mossin, B. L. Tran, D. Adhikari, M. Pink, F. W. Heinemann, J. Sutter, R. K. Szilagyi, K. Meyer and D. J. Mindiola, *J. Am. Chem. Soc.*, 2012, **134**, 13651–13661.

7 (*a*) X. N. Yao, J. Z. Du, Y. Q. Zhang, X. B. Leng, M. W. Yang, S. D. Jiang, Z. X. Wang, Z. W. Ouyang, L. Deng, B. W. Wang and S. Gao, *J. Am. Chem. Soc.*, 2017, **139**, 373–380; (*b*) J. M. Zadrozny, J. Telser and J. R. Long, *Polyhedron*, 2013, **64**, 209–217; (*c*) M. R. Sabera and K. R. Dunbar, *Chem. Commun.*, 2014, **50**, 12266–12269; (*d*) S. Vaidya, A. Upadhyay, S. K. Singh, T. Gupta, S. Tewary, S. K. Langley, J. P. S. Walsh, K. S. Murray, G. Rajaraman and M. Shanmugam, *Chem. Commun.*, 2015, **51**, 3739–3742.

8 (*a*) Y.-Z. Zhang, S. Gómez-Coca, A. J. Brown, M. R. Saber, X. Zhang and K. R. Dunbar, *Chem. Sci.*, 2016, **7**, 6519–6527; (*b*) D. Valigura, C. Rajnak, J. Moncol, J. Titis and R. Boca, *Dalton Trans.*, 2017, **46**, 10950; (*c*) Y.-Y. Zhu, C. Cui, Y.-Q. Zhang, J.-H. Jia, X. Guo, C. Gao, K. Qian, S.-D. Jiang, B.-W. Wang, Z.-M. Wang and S. Gao, *Chem. Sci.*, 2013, **4**,

1802; (*d*) J. Walsh, G. Bowling, A.-M. Ariciu, N. Jailani, N. Chilton, P. Waddell, D. Collison, F. Tuna and L. Higham, *Magnetochemistry*, 2016, **2**, 23; (*e*) M. A. Palacios, J. Nehrkorn, E. A. Suturina, E. Ruiz, S. Gómez-Coca, K. Holldack, A. Schnegg, J. Krzystek, J. M. Moreno and E. Colacio, *Chem. – Eur. J.*, 2017, **23**, 11649; (*f*) J. Li, Y. Han, F. Cao, R. M. Wei, Y. Q. Zhang and Y. Song, *Dalton Trans.*, 2016, **45**, 9279.

9 (*a*) J. Vallejo, A. Pascual-Alvarez, J. Cano, I. Castro, M. Julve, F. Lloret, J. Krzystek, G. De Munno, D. Armentano, W. Wernsdorfer, R. Ruiz-Garcia and E. Pardo, *Angew. Chem., Int. Ed.*, 2013, **52**, 14075–14079; (*b*) L. Chen, J. Wang, Y.-Z. Liu, Y. Song, X.-T. Chen, Y.-Q. Zhang and Z.-L. Xue, *Eur. J. Inorg. Chem.*, 2015, **2015**, 271–278.

10 (*a*) R. C. Poulten, M. J. Page, A. G. Algarra, J. J. Le Roy, I. Lopez, E. Carter, A. Llobet, S. A. Macgregor, M. F. Mahon, D. M. Murphy, M. Murugesu and M. K. Whittlesey, *J. Am. Chem. Soc.*, 2013, **135**, 13640–13643; (*b*) J. Miklovic, D. Valigura, R. Boca and J. Titis, *Dalton Trans.*, 2015, **44**, 12484–12487.

11 (*a*) K. S. Pedersen, M. Sigrist, M. A. Sorensen, A. L. Barra, T. Weyhermuller, S. Piligkos, C. A. Thuesen, M. G. Vinum, H. Mutka, H. Weihe, R. Clerac and J. Bendix, *Angew. Chem., Int. Ed.*, 2014, **53**, 1351–1354; (*b*) J. Martinez-Lillo, T. F. Mastropietro, E. Lhotel, C. Paulsen, J. Cano, G. De Munno, J. Faus, F. Lloret, M. Julve, S. Nellutla and J. Krzystek, *J. Am. Chem. Soc.*, 2013, **135**, 13737–13748.

12 (*a*) Y.-F. Deng, T. Han, Z. Wang, Z. Ouyang, B. Yin, Z. Zheng, J. Krzysteke and Y.-Z. Zheng, *Chem. Commun.*, 2015, **51**, 17688–17691; (*b*) A. Cornia, L. Rigamonti, S. Boccedi, R. Clérac, M. Rouzièresbc and L. Soraced, *Chem. Commun.*, 2014, **50**, 15191–15194.

13 K. S. Pedersen, J. Bendix, A. Tressaud, E. Durand, H. Weihe, Z. Salman, T. J. Morsing, D. N. Woodruff, Y. Lan, W. Wernsdorfer, C. Mathoniere, S. Piligkos, S. I. Klokishner, S. Ostrovsky, K. Ollefs, F. Wilhelm, A. Rogalev and R. Clerac, *Nat. Commun.*, 2016, **7**, 12195.

14 (*a*) L. Chen, J. Wang, J.-M. Wei, W. Wernsdorfer, X.-T. Chen, Y.-Q. Zhang, Y. Song and Z.-L. Xue, *J. Am. Chem. Soc.*, 2014, **136**, 12213–12216; (*b*) L. Chen, S. Y. Chen, Y. C. Sun, Y. M. Guo, L. Yu, X. T. Chen, Z. Wang, Z. W. Ouyang, Y. Song and Z. L. Xue, *Dalton Trans.*, 2015, **44**, 11482–11490.

15 J. Xiang, J.-J. Liu, X.-X. Chen, L.-H. Jia, F. Yu, B.-W. Wang, S. Gao and T.-C. Lau, *Chem. Commun.*, 2017, **53**, 1474–1477.

16 (*a*) D. Shao, S. L. Zhang, L. Shi, Y. Q. Zhang and X. Y. Wang, *Inorg. Chem.*, 2016, **55**, 10859–10869; (*b*) X. C. Huang, C. Zhou, D. Shao and X. Y. Wang, *Inorg. Chem.*, 2014, **53**, 12671–12673; (*c*) F. Habib, I. Korobkov and M. Murugesu, *Dalton Trans.*, 2015, **44**, 6368–6373.

17 (*a*) S. Alvarez, P. Alemany, D. Casanova, J. Cirera, M. Llunell and D. Avnir, *Coord. Chem. Rev.*, 2005, **249**, 1693–1708; (*b*) S. Alvarez, D. Avnir, M. Llunell and M. Pinsky, *New J. Chem.*, 2002, **26**, 996–1009.

18 F. Lloret, M. Julve, J. Cano, R. Ruiz-García and E. Pardo, *Inorg. Chim. Acta*, 2008, **361**, 3432–3445.

19 N. F. Chilton, R. P. Anderson, L. D. Turner, A. Soncini and K. S. Murray, *J. Comput. Chem.*, 2013, **34**, 1164–1175.

20 G. Karlström, R. Lindh, P.-Å. Malmqvist, B. O. Roos, U. Ryde, V. Veryazov, P.-O. Widmark, M. Cossi, B. Schimmelpfennig, P. Neogrady and L. Seijo, MOLCAS: a Program Package for Computational Chemistry, *Comput. Mater. Sci.*, 2003, **28**, 222.